Supporting Information

Douaud et al. 10.1073/pnas.1410378111

SI Materials and Methods

1. Linked ICA.

Participants. In total, 484 right-handed healthy volunteers covering much of the lifespan (age range from 8 to 85 y old; 220 males) were selected from two research projects run by the Research Group for Lifespan Changes in Brain and Cognition at the University of Oslo ("Neurocognitive Development" and "Cognition and Plasticity through the Lifespan"). The study was approved by the Regional Ethical Committee of Southern Norway.

The majority of participants was recruited through newspaper advertisements. Written informed consent was obtained from all participants ≥ 12 y of age and from parents for participants < 18 y of age. Oral informed consent was given by participants < 12 y of age. All subjects were fluent Norwegian speakers and screened using a standardized health interview before inclusion in the study. Exclusion criteria comprised history of self- or parent-reported neurological or psychiatric conditions including stroke, head injury, untreated hypertension, diabetes, use of psychoactive drugs within the last 2 y, and concerns with cognitive status—including memory function. All included MRI scans were examined by a neuroradiologist and deemed free of significant anomalies, including brain tumors and significant vascular insults (stroke).

Imaging acquisition. All participants underwent the same imaging protocol performed using a 12-channel head coil on a 1.5 T Siemens Avanto Scanner (Siemens Medical Solutions) at Oslo University Hospital, Rikshospitalet, with no hardware upgrades and only minor software upgrades performed during the course of the acquisition period (2006–2010). Whole-brain T1-weighted images were acquired using magnetization prepared rapid gradient echo (MPRAGE) with the following parameters: repetition time/echo time/inversion time (TR/TE/TI) = 2,400/3.61/1,000 ms, flip angle of 8°, matrix = 192 × 192, field of view = 240 mm, voxel size of 1.25 × 1.25 × 1.2 mm^3, and 160 sagittal slices. To increase signal-to-noise ratio, the sequence was repeated twice within a single session.

Imaging processing. T1-weighted images were processed using FSL-VBM (1), an optimized voxel-based morphometry protocol (2) using FMRIB Software Library (FSL) tools (3), in which a symmetric study-specific gray matter (GM) template was built from all of the participants' images (fsl.fmrib.ox.ac.uk/fsl/fslwiki/FSLVBM; FSL 4.1.7). For each subject, the input image for FSL-VBM was an average of two repeated MPRAGE sequences. Briefly, the two runs were preprocessed using FreeSurfer, including motion correction, averaging, and intensity nonuniformity correction. Prior to the FSL-VBM processing, the volumes were masked by the full brain-segmented volume output from FreeSurfer (surfer.nmr.mgh.harvard.edu; FreeSurfer 5.0.0) (4), effectively excluding nonbrain compartments. After nonlinearly registering all of the brain-extracted, GM-segmented images onto the symmetric study-specific GM template, the optimized FSL-VBM protocol involved a compensation (or "modulation") for the local contraction/enlargement caused by the nonlinear component of the transformation: each voxel of each registered GM image was multiplied by the Jacobian of the warp field. The modulated registered GM-segmented images were then smoothed with an isotropic Gaussian kernel with a σ of 4 mm (~9.4 mm full width at half maximum).

In addition, brain structural information was also derived from two other complementary types of GM image processing: vertexwise cortical thickness and surface area measures calculated using FreeSurfer by means of an automated surface reconstruction scheme (4).

Linked ICA. Linked ICA is an entirely data-driven approach that can comodel multiple imaging modalities. Its main goal is to model the imaging data as a set of interpretable features (independent components), most of them characterizing biophysically plausible modes of variability across all subjects' images. Unlike in a principal component analysis, the mixing matrix vectors of an ICA are not forced to be orthogonal to each other, and thus can explain common variance of variables external to the ICA, such as age. Linked ICA is implemented as described in detail in earlier papers (5, 6) (http://fsl.fmrib.ox.ac.uk/fsl/fslwiki/FLICA). We ran the linked ICA decomposition with 70 components to make it comparable with the work by Smith et al. (7). Linked ICA is capable of eliminating unneeded components (using Bayesian model order selection), but in all cases here, it kept all components.

2. Components Showing Relationship with Age. For the purpose of this study, we focused on components showing relationship with age (as assessed using a quadratic fit). There were eight such components, but only two achieved statistical as well as clear practical significance: IC1 and IC4 (significance measured using effect magnitude as opposed to P values) (Fig. 1) (8). The first such component (IC1) was the expected global dominant mode showing monotonic decrease of the whole GM with age (except for the medial temporal lobe). The weight for this IC1 component was essentially composed of GM volume information (42%) and cortical thickness (51%), and only very modestly of cortical area (7%). In contrast, the other component (IC4) showed a nonmonotonic relationship with age, describing a symmetric inverted-U shape with age with the strongest quadratic coefficient of all age-related components. The weight for this IC4 component was largely carried by GM volume information (53%) rather than thickness (20%) or area (23%), and the latter two contributions did not survive a threshold of $Z > 4$. In the opposite contrast (i.e., decreasing in early age and increasing in older age), cortical thickness showed a strong effect in the anterior and ventral medial cingulate cortex and the insula (nonoverlapping with volume effects) and volume effects in the inferior temporal gyrus. This somewhat surprising result is actually in line with what Salat et al. (9, 10) have consistently observed with aging in the anterior cingulate cortex and the inferior temporal gyrus, and might be related to a change in intensity and contrast in these specific brain areas, for which the histological mechanism are unclear.

The best fit for the relationship between this second component IC4 and age was quadratic ($P = 6 \times 10^{-73}$) in the shape of an inverted U with a peak at 40.2 y: $y = -0.00182x^2 + 0.14643x - 2.00964$ (norm of residuals = 15.57; goodness of fit: sum of squared errors (SSE) = 242.5; adjusted $R^2 = 0.50$; MATLAB7.12). A cubic fit showed no substantial improvement (norm of residuals = 15.53). Quadratic models also provided a good fit for the relationship between the second age-related component IC4 and age for males and females taken separately (Fig. S4). We tested for a difference in the peak of the curves between males ($n = 224$) and females ($n = 260$) in age and height using bootstrap resampling with replacement: we computed this difference based on separate quadratic fits for two populations of same size ($n = 224$ and $n = 260$), both of them randomly sampled from the entire healthy population of $n = 484$ (10,000 iterations). The peak of the curve was significantly higher and later for females than males at 40.9 y for females compared with 38.8 y for males ($P < 10^{-4}$ and $P = 4.5 \times 10^{-3}$, respectively).

There was a nonmonotonic inverted-U relationship between the two age-related components IC1 and IC4 that was fully driven

by their strong relationships to age (as age explained 90% of the variance of the dominant age-related component IC1 and 50% of the variance of the second age-related component IC4); when the modeled age-quadratic effect was removed from both components, their residuals showed no relationship.

3. Comparison with Alzheimer's Disease and Adolescent-Onset Schizophrenia.

Participants. The Alzheimer's disease (AD) cohort comprised 62 healthy controls and 58 AD patients (overall mean age = 73 ± 8 y). Subjects' demographics, and inclusion/exclusion and diagnosis criteria, have been previously described (11). The 120 participants underwent the same imaging protocol on a 3 T Allegra MR Imager (Siemens) with a standard quadrature head coil and maximum 40 $mT.m^{-1}$ gradient capability. This imaging protocol included whole-brain T1-weighted scanning using MPRAGE with the following parameters: TR/TE/TI = 2,150/3.49/1,000 ms, flip angle of 7°, field of view = 280 mm, voxel size of 1.1 mm isotropic, and 144 sagittal slices. Structural scans were processed using the optimized FSL-VBM protocol (smoothing with 3-mm σ-Gaussian kernel) (1), and *t* maps representing group differences between patients and controls were generated.

For the adolescent-onset schizophrenia (AOS) comparison included here, 12 healthy controls and 12 AOS patients were considered (mean age at baseline = 16.0 ± 1.5 y). Subjects' demographics, inclusion/exclusion criteria, medication, imaging protocol, and results have been previously described in detail (12). Structural scans at baseline and a second time point (2.5 y later) were reprocessed using the same FSL-VBM protocol as for the 484 healthy participants and the 120 subjects of the AD study (1). The modulated registered GM images from the second time point were subtracted from those at baseline, and the resulting images were smoothed with an isotropic Gaussian kernel with a σ of 4 mm, and *t* maps representing between-group (patients vs. controls) differences in these changes over time were generated.

Spatial cross-correlation. We compared the spatial distribution of the inverted-U component IC4 and the pattern of abnormalities in AD and AOS using voxel-by-voxel spatial cross-correlation in FSL 5.0.5 (3). For this analysis, we first used a nonlinear registration from the average GM map across all 120 elderly participants of the AD cohort onto the average GM map across all 484 healthy participants and applied the warpfield to the map of structural abnormalities in AD. We carried out the same procedure for the AOS cohort. The reason for this step is that, although all images are in the Montreal Neurological Institute (MNI) space, each cohort will be in its own study-specific standard space, as is required by the optimized VBM protocol. As a consequence, the standard space template for the AOS cohort will, for instance, display much smaller ventricles than the one for the AD cohort. Then, we masked each map with the MNI152 brain mask and correlated all voxels of the inverted-U component ($Z > 0$) with the statistical map of regions showing lower volume in AD compared with their matched controls ($t > 0$), and those regions showing late development in AOS compared with matched healthy adolescents ($t > 0$).

To assess the significance of the spatial cross-correlation between the spatial distribution of the inverted-U component IC4 and maps of both AD and AOS structural abnormalities, we randomly generated 1,000 Gaussian noise images that we smoothed with the corresponding estimated smoothness for AD and AOS differences with their respective controls. We then calculated the 1,000 cross-correlations between each of these noise maps and the network corresponding to the inverted-U component and compared the strength of our observed correlations with this empirically generated null distribution.

Prediction of AOS and AD. We spatially regressed the GM network corresponding to the inverted-U component IC4 ($Z > 0$) into the GM volume images of each AD patient and matched control, as well as each AOS patient and matched control. We then used this single measure for each subject to calculate the specificity, sensitivity, and accuracy of prediction of the two clinical disorders using a linear discriminant analysis and leave-one-out cross-validation in datamind (R) (13).

Post hoc correlation with cognitive measures in healthy subjects. Finally, we wanted to investigate post hoc the relationship between the strength of the inverted-U component IC4 and two cognitive measures that are hallmarks of AD and AOS: episodic memory (as assessed with the CVLT long-delay free recall) and the performance (fluid) and verbal (crystallized) intelligence raw scores (block design and vocabulary; WASI) (Figs. 4 and 5). For verbal (crystallized) intelligence, which is known to plateau, we also considered only values for the 249 of 484 healthy participants who were under 40 y old, the peak age for the inverted-U component (Fig. S5). We further assessed if any of these measures still correlated significantly with the inverted-U component strength after regressing out the linear and quadratic effect of age using the linear model in R. All of the correlations survived correction for multiple comparisons across all components and were still significant after correction for linear effect of age, but not for a quadratic effect of age, as lifespan trajectories for fluid intelligence, episodic memory, and inverted-U component were very similar (Fig. S6). For completeness, we compared the correlation values between these cognitive measures and all age-related components (Fig. S2).

1. Douaud G, et al. (2007) Anatomically related grey and white matter abnormalities in adolescent-onset schizophrenia. *Brain* 130(Pt 9):2375–2386.
2. Ashburner J, Friston KJ (2000) Voxel-based morphometry—the methods. *Neuroimage* 11(6 Pt 1):805–821.
3. Smith SM, et al. (2004) Advances in functional and structural MR image analysis and implementation as FSL. *Neuroimage* 23(Suppl 1):S208–S219.
4. Fischl B, et al. (2002) Whole brain segmentation: Automated labeling of neuroanatomical structures in the human brain. *Neuron* 33(3):341–355.
5. Groves AR, Beckmann CF, Smith SM, Woolrich MW (2011) Linked independent component analysis for multimodal data fusion. *Neuroimage* 54(3):2198–2217.
6. Groves AR, et al. (2012) Benefits of multi-modal fusion analysis on a large-scale dataset: Life-span patterns of inter-subject variability in cortical morphometry and white matter microstructure. *Neuroimage* 63(1):365–380.
7. Smith SM, et al. (2009) Correspondence of the brain's functional architecture during activation and rest. *Proc Natl Acad Sci USA* 106(31):13040–13045.
8. Kirk RE (1996) Practical significance: A concept whose time has come. *Educ Psychol Meas* 56(5):746–759.
9. Salat DH, et al. (2004) Thinning of the cerebral cortex in aging. *Cereb Cortex* 14(7):721–730.
10. Salat DH, et al. (2009) Age-associated alterations in cortical gray and white matter signal intensity and gray to white matter contrast. *Neuroimage* 48(1):21–28.
11. Douaud G, et al. (2011) DTI measures in crossing-fibre areas: Increased diffusion anisotropy reveals early white matter alteration in MCI and mild Alzheimer's disease. *Neuroimage* 55(3):880–890.
12. Douaud G, et al. (2009) Schizophrenia delays and alters maturation of the brain in adolescence. *Brain* 132(Pt 9):2437–2448.
13. Duchesnay E, et al. (2007) Classification based on cortical folding patterns. *IEEE Transactions on Medical Imaging* 26(4):553–565.

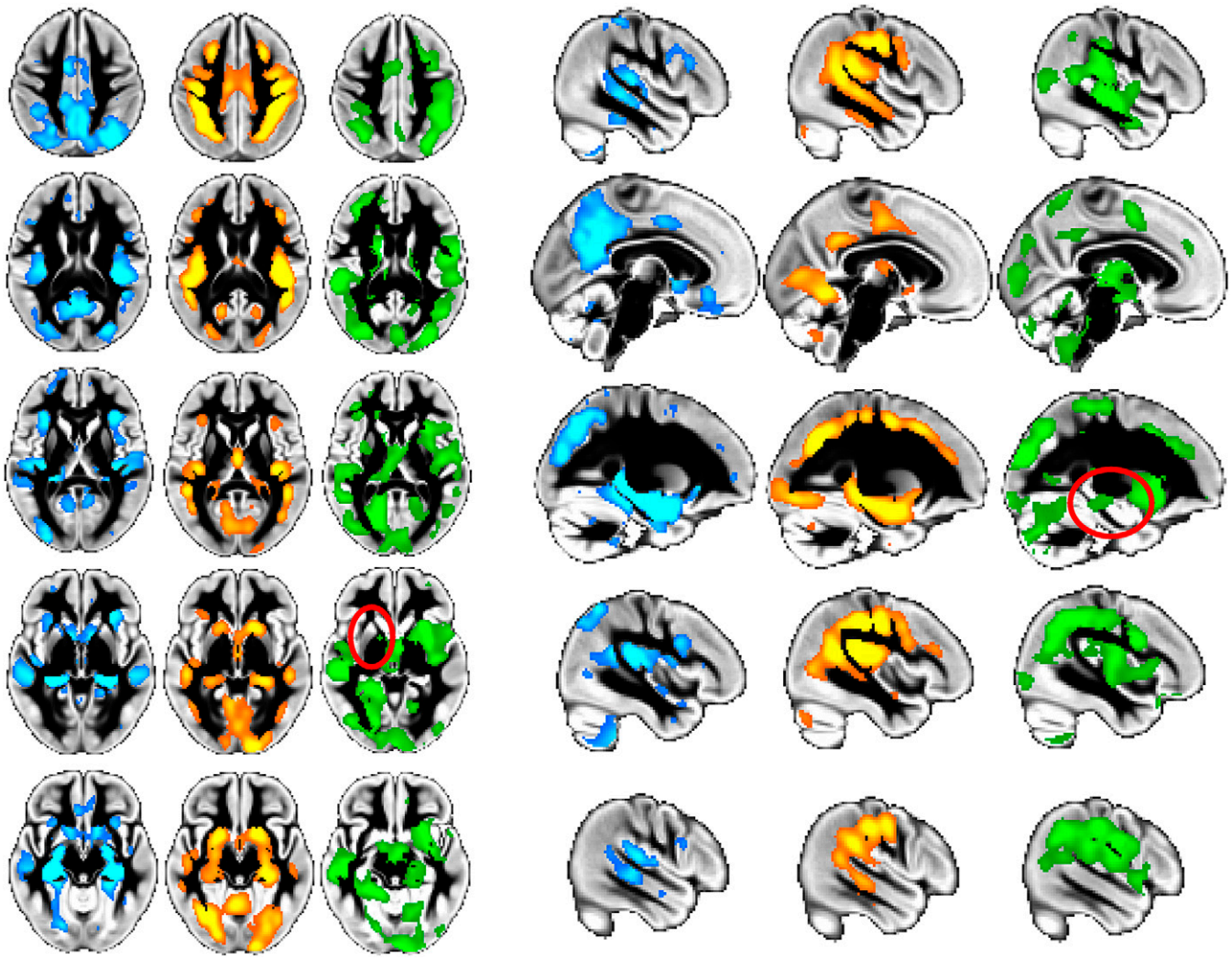

Fig. S1. AD-related abnormalities, the spatial network of the inverted-U component, and AOS-related abnormalities spatially correspond to one another. (*Left*) Axial and (*Right*) sagittal slices showing AD-related abnormalities (blue; thresholded for better visualization at $P < 0.001$), the spatial network of the inverted-U component IC4 (orange; $Z > 4$), and AOS-related abnormalities (green; $P < 0.05$). Main differences are the lack of extensive structural abnormalities in the medial temporal lobe as well as some apparent asymmetry in AOS (red ovals).

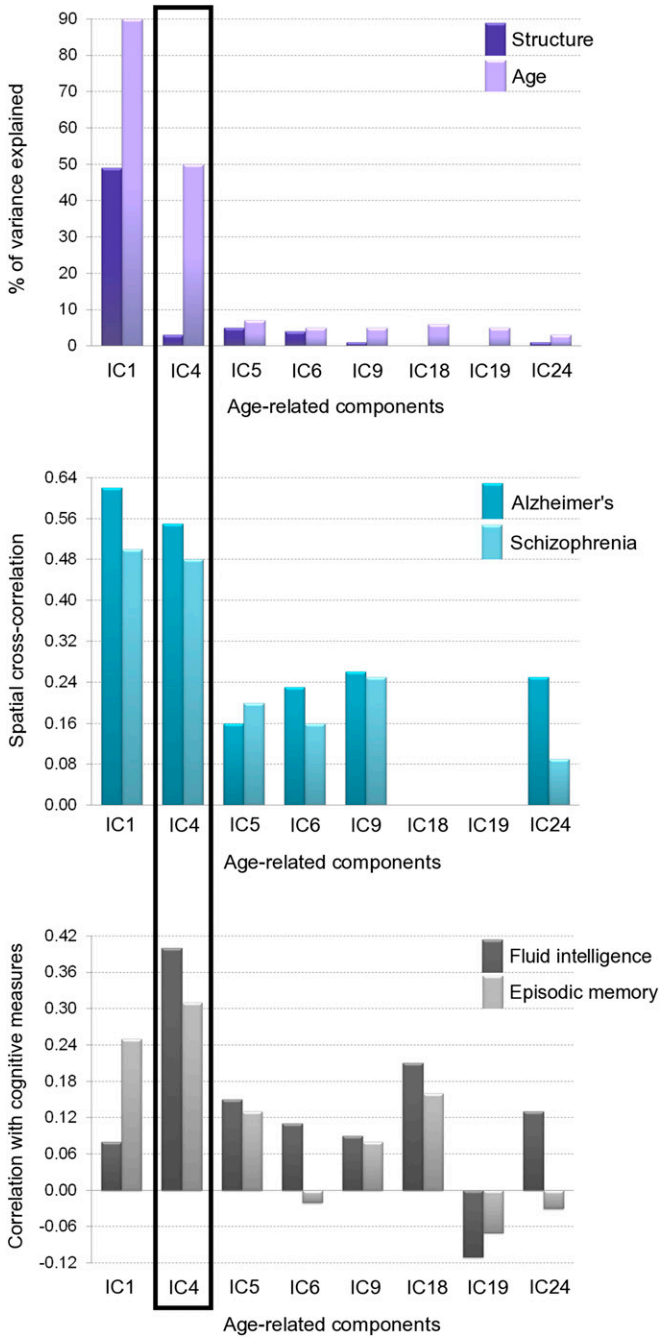

Fig. S2. Characteristics of age-related components. (*Top*) For each of eight components that were significantly related to age (quadratic fit), we measured across all 484 healthy subjects (*i*) the percentage of variance of GM volume ("structure") that the component explained and (*ii*) the percentage of variance within that component explained by age (Fig. 1). Of note, although the inverted-U component (IC4) accounted for only 3% of the variance of GM volume (structure), 50% of the variance within the IC4 component was associated with age. (*Middle*) Spatial cross-correlations between the GM volume map for each age-related component and AD/AOS structural abnormalities: both IC1 (the global component mostly representing the standard deviation of GM volume across all of the subjects) and IC4 (the age-related inverted-U component mostly representing transmodal areas) were highly correlated with AD and AOS spatial distribution of abnormalities. (*Bottom*) Correlations with fluid intelligence (block design; not age-corrected) and episodic memory (CVLT long-delay recall; not age-corrected); across the lifespan and all healthy participants, IC4 had the strongest correlations with both cognitive measures.

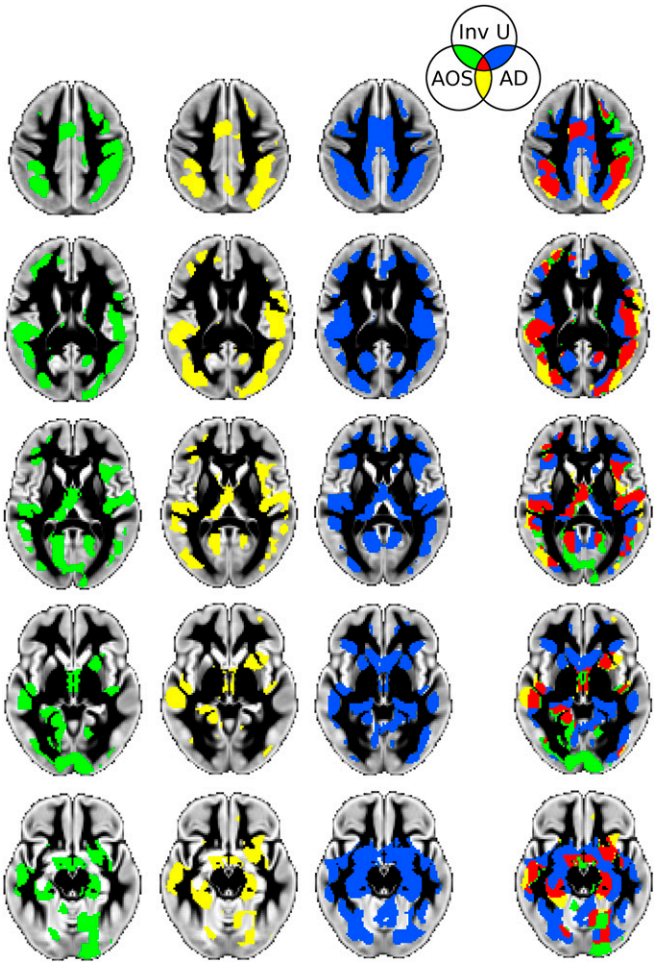

Fig. S3. Binary overlaps show spatial commonality between the pattern of the inverted-U component and the pattern of abnormalities in AD and AOS. In green is the overlap between the inverted-U component IC4 and AOS, in yellow is the "disease" overlap between AD and AOS, and in blue is the overlap between the inverted-U component IC4 and AD (arbitrary threshold at $P < 0.05$). In red is the overlap between all three patterns. The most notable differences are the lack of extensive abnormalities in the amygdalo-hippocampal complex in AOS (see also the main text). Inv U, inverted-U.

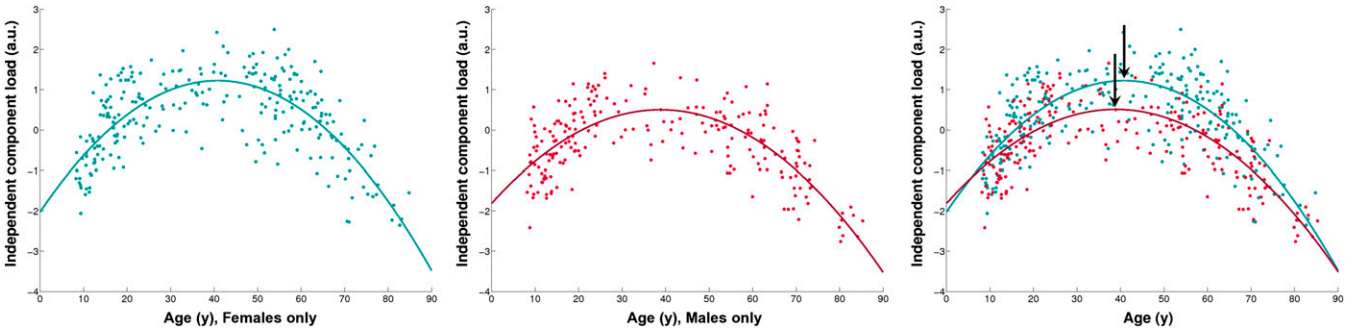

Fig. S4. Inverted-U component load differs between females and males. (*Left*) Inverted-U component IC4 load for all females (turquoise; $n = 260$) and (*Center*) all males (magenta; $n = 224$) plotted against age. (*Right*) A quadratic model provided an excellent fit for the relationship between the component load and age for females ($P = 3.5 \times 10^{-44}$) and males ($P = 1.3 \times 10^{-33}$) taken separately, with a higher, slightly later peak for the females than for the males (black arrows; $P = 4.5 \times 10^{-3}$): females $y_F = -0.00195x_F^2 + 0.15919x_F - 2.0271$; males $y_M = -0.00154x_M^2 + 0.11936x_M - 1.8158$. a.u., arbitrary unit.

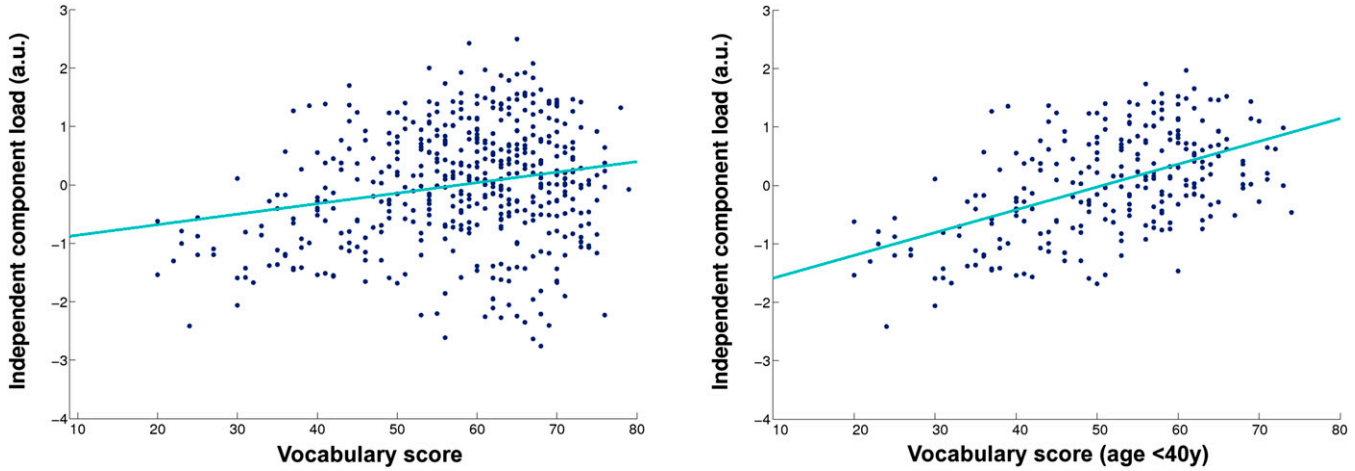

Fig. S5. Inverted-U component load correlates with crystallized intelligence scores in healthy subjects. Crystallized intelligence, in contrast to episodic memory and fluid intelligence, does not peak with age, but instead reaches a plateau. Estimates for this age plateau vary depending on whether they are made, for instance, from cross-sectional or longitudinal data (similar to what has been observed for age peaks in fluid intelligence and episodic memory) (1–3), usually from 25–35 to 45–55 y. We therefore looked at the correlation between the inverted-U component IC4 load and one measure of crystallized intelligence (vocabulary; WASI) not only across all participants, but also for participants under 40 y old, which corresponds to the peak of the inverted U. (*Left*) For all healthy participants ($n = 481$; $r = 0.21$; $P = 2.6 \times 10^{-6}$). (*Right*) Stronger correlation was seen for all healthy participants under 40 y old ($n = 249$; $r = 0.52$; $P = 4.9 \times 10^{-19}$). a.u., arbitrary unit.

1. Rönnlund M, Nyberg L, Bäckman L, Nilsson LG (2005) Stability, growth, and decline in adult life span development of declarative memory: Cross-sectional and longitudinal data from a population-based study. *Psychol Aging* 20(1):3–18.
2. Ronnlund M, Nilsson LG (2006) Adult life-span patterns in WAIS-R Block Design performance: Cross-sectional versus longitudinal age gradients and relations to demographic factors. *Intelligence* 34(1):63–78.
3. Craik FI, Bialystok E (2006) Cognition through the lifespan: Mechanisms of change. *Trends Cogn Sci* 10(3):131–138.

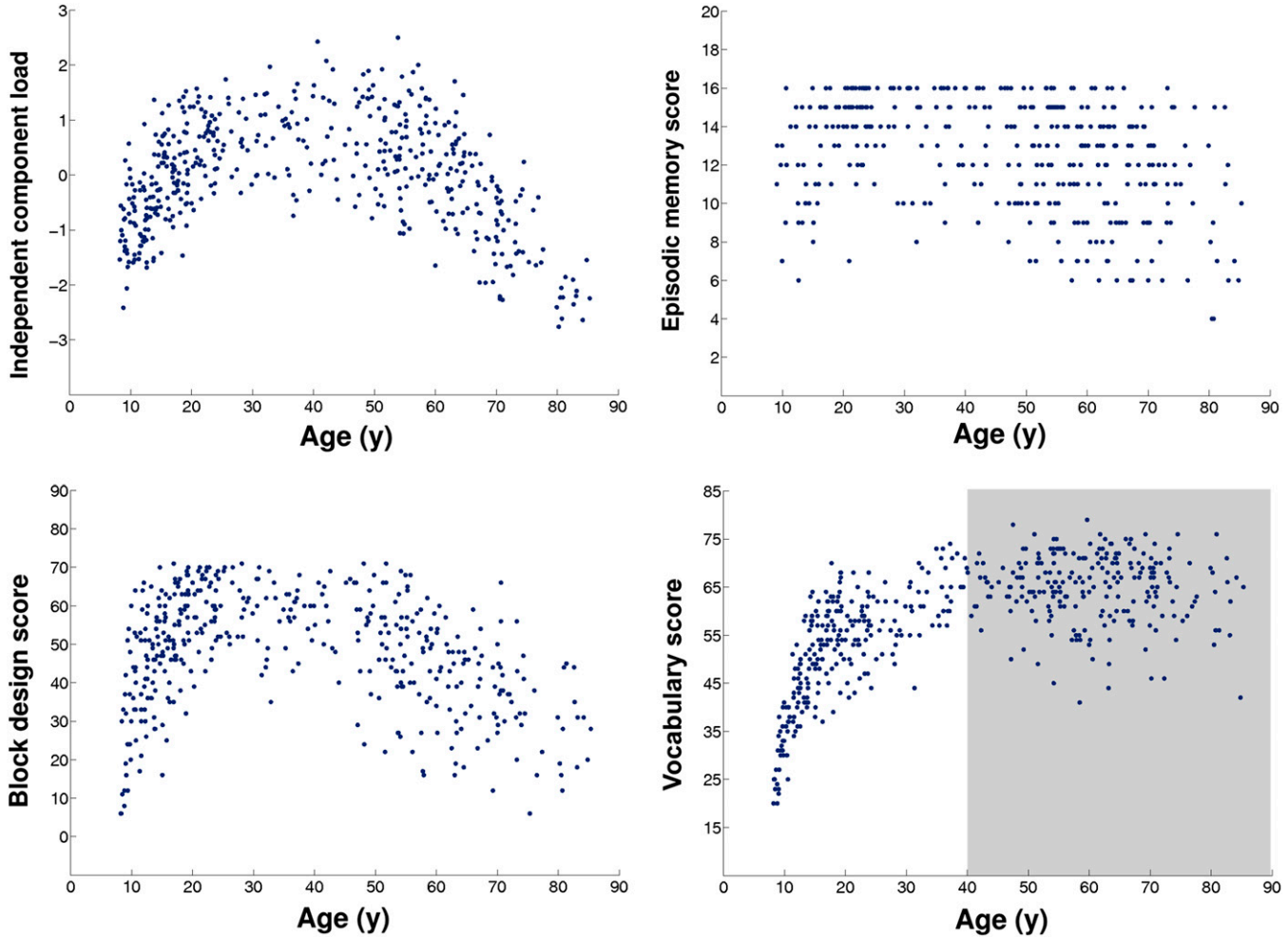

Fig. S6. Similar lifespan trajectories for the inverted-U component, long-term memory, and fluid and crystallized intelligence (<40 y). There were similar inverted-U quadratic relationships between age and inverted-U component IC4 (peaking at 40 y), episodic memory scores (peaking at 32 y), and block design scores (peaking at 38 y). Age trajectory of vocabulary scores before 40 y (when it crystallizes to a plateau) also matched that of the inverted-U component for the same age range (Fig. S5).

Table S1. MNI coordinates of local maxima for the GM network corresponding to the inverted-U component ($Z > 4$)

Cortical region [Brodmann Area (BA)]	Side	MNI (voxel)			*Z* value
		x	*y*	*z*	
Medial temporal areas					
Amygdalohippocampal complex	Left	59	62	26	8.74
Amygdalohippocampal complex	Right	32	61	27	8.91
Dentate gyrus	Left	58	47	32	8.04
Other temporal areas					
Posterior superior temporal sulcus	Left	69	48	35	6.24
Posterior superior temporal sulcus	Right	21	48	35	6.66
Temporoparietal areas					
Supramarginal/angular gyrus	Left	68	39	44	9.78
Supramarginal/angular gyrus	Right	21	41	42	8.17
Parietal areas					
Intraparietal sulcus (anterior)	Right	28	38	56	13.89
Intraparietal sulcus (anterior)	Left	64	46	57	12.12
Intraparietal sulcus (posterior)	Left	58	31	54	12.12
Intraparietal sulcus (posterior)	Right	32	31	54	10.33
Other parietal areas					
Posterior cingulate cortex	Right	40	40	53	7.73
Posterior cingulate cortex	Left	50	39	53	7.56
Parieto-occipital fissure (precuneus)	Left	53	29	51	8.68
Parieto-occipital fissure (precuneus)	Right	37	29	49	8.16
Opercular/insular areas					
Parietal operculum	Left	65	50	44	13.45
Parietal operculum	Right	26	53	44	9.17
Frontal operculum/anterior insula	Right	28	77	38	5.10
Prefrontal areas					
Middle frontal gyrus (BA9)	Right	26	67	52	10.28
Middle frontal gyrus (BA9)	Left	64	66	52	9.19
Middle frontal gyrus (BA46)	Left	65	77	46	6.56
Middle frontal gyrus (BA46)	Right	25	78	45	4.99
Superior frontal gyrus (BA8)	Right	33	71	59	7.47
Superior frontal gyrus (BA8)	Left	57	72	58	7.54
Superior frontal gyrus (BA6)	Right	32	60	61	8.32
Superior frontal gyrus (BA6)	Left	59	60	60	7.93
Medial superior frontal gyrus (BA6)	—	45	57	62	6.44
Other frontal areas					
Precentral gyrus (BA4)	Left	65	55	58	9.85
Precentral gyrus (BA4)	Right	26	54	58	9.46
Occipital areas					
Calcarine fissure	Left	52	14	34	9.24
Lateral occipital cortex	Left	66	30	38	6.57
Lateral occipital cortex	Right	23	33	36	5.03
Lingual gyrus	—	45	24	37	6.62
Lingual gyrus	Right	40	34	38	6.17
Temporo-occipital areas					
Fusiform gyrus	Right	28	30	29	9.12
Fusiform gyrus	Left	61	30	30	5.72
Cerebellum					
Crus I	Right	23	25	21	5.15
Crus I	Left	67	25	21	4.14
I–IV	—	43	35	32	7.85
Subcortical areas					
Ventral striatum	Left	54	69	33	9.79
Ventral striatum	Right	35	68	32	9.18
Thalamus	—	45	57	41	7.79

Regions were identified based on the Harvard–Oxford in vivo probabilistic atlas, the Jülich cytoarchitectonic probabilistic atlas, and the probabilistic cerebellar atlas available in FSL.